The HYPERMAQ dataset: bio-optical properties of moderately to extremely turbid waters

Héloïse Lavigne[1], Ana Dogliotti[2], David Doxaran[3], Fang Shen[4], Alexandre Castagna[5], Matthew Beck[1], Quinten Vanhellemont[1], Xuerong Sun[4], Juan Ignacio Gossn[2,7], Pannimpullath Remanan Renosh[3], Koen Sabbe[5], Dieter Vansteenwegen[6], Kevin Ruddick[1]

[1] Royal Belgian Institute of Natural Sciences, Brussels, Belgium
[2] Instituto de Astronomía y FísicadelEspacio (IAFE), CONICET-Universidad de Buenos Aires, Buenos Aires, Argentina
[3] Laboratoire d'Océanographie de Villefranche, UMR7093 Sorbonne Université /CNRS, Villefranche-sur-Mer, France
[4] State Key Laboratory of Estuarine and Coastal Research (SKLEC), East China Normal University, Shanghai, China
[5] Laboratory of Protistology and Aquatic Ecology, Ghent University, Ghent, Belgium
[6] Flanders Marine Institute (VLIZ), Ostend, Belgium
[7] European Organisation for the Exploitation of Meteorological Satellites (EUMETSAT),Darmstadt, Germany.

Correspondence to: Héloïse Lavigne (hlavigne@naturalsciences.be)

Abstract. Because of the large diversity of case 2 waters ranging from extremely absorbing to extremely scattering waters and the complexity of light transfer due to external terrestrial inputs, retrieving main biogeochemical parameters such as chlorophyll-a or suspended particulate matter concentration in these waters is still challenging. By providing optical and biogeochemical parameters for 180 sampling stations with turbidity and chlorophyll-a concentration ranging from 1 to 700 FNU and from 0.9 to 180 mg m^{-3} respectively, the HYPERMAQ dataset will contribute to a better description of marine optics in optically complex water bodies and can help the scientific community to develop algorithms. The HYPERMAQ dataset provides biogeochemical parameters (i.e. turbidity, pigment and chlorophyll-a concentration, suspended particulate matter), apparent optical properties (i.e. water reflectance from above water measurements) and inherent optical properties (i.e. absorption and attenuation coefficients) from six different study areas. These study areas include large estuaries (i.e. the Rio de la Plata in Argentina, the Yangtze Estuary in China and the Gironde Estuary in France), inland (i.e. the Spuikom in Belgium and Chascomùs lake in Argentina) and coastal waters (Belgium).The dataset is available from Lavigne et al (2022), https://doi.pangaea.de/10.1594/PANGAEA.944313.

1 Introduction

In marine optics, certain water properties such as the concentration of chlorophyll-a ([Chl-a] hereafter) or suspended particulate matter (SPM hereafter) are inferred from water leaving reflectance allowing a powerful satellite-based monitoring. However, although algorithms are well matured in clear case 1 waters (Morel and Prieur, 1975; Morel and Maritorena, 2001), it is not the case in optically complex case 2 waters where apparent optical properties (AOPs) and inherent optical properties (IOPs) are influenced not only by [Chl-a] but also by terrestrial

optically-active substances such as suspended sediments and colored dissolved organic matter (CDOM) that do not covary with [Chl-a]. Given the complexity of light transfer in these waters and the large diversity of case 2 waters, algorithm definition is much more challenging (Odermatt et al., 2012) and requires datasets covering the extreme variability of case 2 water conditions. Hence, additional data obtained in optically complex waters are valuable to the scientific community as they will help to better understand marine optics in such waters and to design ocean color algorithms.

The present dataset (Lavigne et al., 2022; https://doi.pangaea.de/10.1594/PANGAEA.944313) has been collected as part of the HYPERMAQ project. During this project, different types of optically complex waters with turbidity ranging from moderate to extreme (1 to 700 FNU) and [Chl-a] ranging from low to very high (0.9 to 180 mg m^{-3}) have been sampled in various locations around the world. Their main optical and biogeochemical parameters are shared in this dataset, including measurements of water-leaving reflectance, turbidity, non-water light absorption and attenuation coefficients as well as SPM, [Chl-a] and other pigment composition. In the next sections, study areas, sampling methodology and final HYPERMAQ datasets are described.

2 Sites

Contrary to case-1 waters, optical properties of case-2 waters are impacted by terrestrial inputs of sediments and CDOM with concentrations ranging from low to extreme values. Hence, in these waters, the retrieval of water properties from bio-optical algorithms is extremely complex. As case-2 waters are generally highly connected to land-ocean interaction and human activities (estuaries, coastal and inland waters), it becomes critical to collect enough in situ data to help for the development of specific algorithms. Given the large diversity of case-2 waters, Hieronymi et al. (2016) defined four main groups: case-2 scattering (C2S), case-2 extremely scattering (C2SX), case-2 absorbing (C2A) and case-2 extremely absorbing (C2AX), suggesting that specific efforts in algorithm development should be given to each group. For instance, Hieronymi et al. (2017) proposed a multi-neural networks algorithm for case-2 waters atmospheric correction, but the algorithm was mostly trained and validated with synthetic datasets. In this context, the HYPERMAQ dataset provides bio-optical data from C2S and C2SX waters by sampling a very large diversity of waters affected by additional sediments inputs (see sample sites on Figure 1). Sample sites allow obtaining a large range in SPM and turbidity (1 to 700 FNU) by sampling Belgian coastal waters which are extremely turbid locally close to the coast and less turbid further offshore. In addition, three estuaries known to be extremely turbid have been sampled (the Gironde (France), the Yangtze (China) and the Rio de la Plata (Argantina) estuaries). Since they are affected by tides, a gradient of turbidity could be sampled along the day with diverse influences of oceanic waters. These three estuaries, located on different continents, carry suspended particles with their own mineral properties, enriching then the database. Finally, two terrestrial lagoons were sampled. One with low to moderate concentrations in suspended sediments (Spuikom in Belgium) and one with extreme concentrations of both algae and non-algal suspended particles (Chascomùs in Argentina). This large diversity of sampled sites should then help to improve our knowledge of case-2 moderately to extremely scattering waters. A detailed description of each site is provided below.

2.1 Belgian coastal waters

The Belgian coastal waters (latitudes:51.27° to 51.59°N; longitudes: 2.50° to 3.15°E) have been sampled in April 2018 and July 2018 from the RV Simon Stevin (Table 1). Belgian coastal waters are dominated by Atlantic waters which enter from the English Channel (Lacroix et al., 2004) and experience very strong along shore tidal currents which cause sediment resuspension leading to high turbidity. SPM concentrations range from less than 1 g m^{-3} in offshore and deeper waters to more than 100 g m^{-3} in very shallow waters. Phytoplankton blooms, characterized by high [Chl-a] concentration (more than 10 mg m^{-3}), develop in spring from March to May. During summer, the biomass remains rather high (5 to 10 mg m^{-3}) compared to winter when phytoplankton growth is mostly limited by light (Lancelot et al., 2005). The blooming season is mostly dominated by two taxa: diatoms in early spring and summer and *Phaeocystis globosa* in April-May (Muylaert et al., 2006).

2.2 Spuikom lagoon

The Spuikom lagoon (latitude: 51.23°N, longitude: 2.95°E) is an artificial basin that is connected to Ostend harbor (Belgium) by a lock system. The Spuikom has a surface area of 0.82 km^2 and an average depth of 1.5 m. In the past, it has been used as a flushing basin to flush sediments from the harbor channel. Today it is used for leisure and commercial activities like sailing and shellfish farming. The Spuikom can experience events of phytoplankton blooms, of high turbidity (when strong winds cause the resuspension of bottom sediments), and of clear waters, which allow the development of microphytobenthic biofilms and macroalgae in the bottom (Castagna et al., 2022). The system was sampled during the growth season of 2018 (April and July, Table 1). Measurements were performed from inflatable boats provided by Ghent University and VLIZ (Zeekat).

2.3 Gironde Estuary

The Gironde Estuary, southwest France, is a good example of sediment-dominated case 2 waters influenced by river inputs. The Gironde Estuary has been sampled between 17-20 September 2018 in two locations: Pauillac (latitude: 45.1975°N, longitude: -0.7422°E) close to the maximum turbidity zone and Le Verdon (latitude: 45.5438°N, longitude: -1.042°E) close to the river mouth. In the Gironde Estuary, the origin of the particles is twofold: inputs from rivers Garonne and Dordogne anderosion of recently settled sediments by tidal currents (Castaing and Allen, 1981). The suspended matter is a mixture of organic and mineral composites, where the organic fraction represents less than 2% of the total material (Doxaran et al. 2002). The mineral fraction is composed of micas (63%) and quartz (25%), while clay phases contain four minerals: montmorillonite (30%), illite and interstratified minerals (40%), kaolinite (15%), chlorite and interstratified minerals (15%). [Chl-a] and CDOM concentrations are low, with [Chl-a] ranging from 1 to 3 mg m^{-3} (Irigoien & Castel, 1997), and dissolved organic carbon (DOC) ranging from 1 to7 mgC L^{-1} (Abril et al., 1999; Castaing and Allen, 1981). The Gironde Estuary has well-developed turbidity maximum zones, with both tidal asymmetry and density residual circulation involved in their formation (Castaing and Allen,1981). It is characterized by SPM concentrations ranging from 10 to 1000 g m^{-3} within surface waters (Doxaran et al. 2009a).

108 **2.4 Chascomús lake**

109 Chascomús lake, located in the Pampa Plain in the Buenos Aires Province in Argentina (latitude: -35.5828°N,

110 longitude: -58.0202°E), with a surface area of ~ 30 km^2, is a highly turbid, shallow lagoon (average depth of ~ 1.9

111 m), permanently mixed due to intense and persistent winds (Torremorell et al., 2007). Total suspended matter

112 varies widely from 66.3 to 614 g m^{-3} with a mean value of 227.3 ±133.7 g m^{-3} (Diovisalvi et al. 2014) and on

113 average the inorganic content represented ~65%. Nephelometric turbidity also widely ranged from 76.46 to 509.74

114 NTU, with a mean value of 209.18±112.76 NTU. Turbidity was highly correlated to SPM while no significant

115 correlation with [Chl-a] was found (Pérez et al. 2011). Total [Chl-a] concentration ranged from 50.6 to 856.3 mg

116 m^{-3} (mean = 328.5 ±173.4 mg m^{-3}) during the 2005-2009 sampled period (Diovisalvi et al. 2014). The lake is

117 characterized by high primary production (Torremorell et al., 2009) and a rich and diverse phytoplankton commu-

118 nity, mostly composed of cyanobacteria. In terms of biovolume, cyanobacteria contribute 50% to total phytoplank-

119 ton biovolume and 75% to total C in the water column (Diovisalvi et al. 2010). Despite the high CDOM absorption

120 (a_{CDOM}, mean $a_{CDOM}(440)$=4.65 ± 0.91 m^{-1}), absorption by particulate fraction (a_p) has a prominent role in light

121 absorption, for which both phytoplankton pigments (a_{phy}) and non-pigmented particles (a_{NAP}) contribute similarly

122 to total particulate absorption (Pérez et al. 2011). Both SPM (especially the inorganic part) and [Chl-a] (less pro-

123 nounced) show seasonal variation with increasing values in spring and summer (Mid-September to Mid-March),

124 while the dissolved fraction did not show a significant seasonal difference (Pérez et al. 2011). The HYPERMAQ

125 field campaign in Chascomús lake took place on 9-10 April 2018. Radiometric, in-water measurements as well as

126 samples were collected at the end of a 164 m long pier.

127 **2.5 Río de la Plata**

128 The Río de la Plata is a large and shallow funnel shaped estuary with high values SPM, ranging from 100 to 300

129 g m^{-3} (Framiñan and Brown, 1996) and reaching 940 g m^{-3} in the maximum turbidity zone (Dogliotti et al. 2014).

130 Turbidity values widely vary between 2 and 680 FNU (Dogliotti et al. 2016). SPM, turbidity and [Chl-a] spatial

131 distribution and temporal variability is highly variable. In the upper estuary, a freshwater with tidal regime area,

132 turbidity increases from January to April/May (with higher values along the southern Argentinian coast compared

133 to the northern Uruguayan coast), and decreases from June to September (Dogliotti et al. 2016). In turn [Chl-a]

134 also show high spatial variability, in the upper estuary higher values are generally found in the northern part (Uru-

135 guay) compared to the southern part (Argentina). In particular, high [Chl-a] have been recorded during spring-

136 summer months related to cyanobacteria blooms both along the Uruguay (Aubriot et al. 2020) and Argentine

137 (Dogliotti et al. 2021) coasts, when [Chl-a] values as high as 13.6 and 153 mg m^{-3} have been recorded, respectively.

138 Measurements in the Rio de la Plata were performed from a fixed 500 m long pontoon at the Palermo Pescadores

139 Club in Buenos Aires (latitude: -34.5609°N, longitude: -58.3988°E) on 4 and 5 April 2018.

140 **2.6 Yangtze Estuary**

141 The Yangtze Estuary is located on the east coast of China and close to East China Sea (Figure 1). Influenced by

142 the Yangtze River, the largest river in China and the third largest in the world due to its enormous runoff, which

143 discharges an annual average of 9×10^{11} m^3 of freshwater and 4×10^8 tons of sediment into the estuary from 1950s

144 to 2000 (Chen et al., 2003), the Yangtze Estuary is an extremely turbid area (Shen et al., 2010a). Taking 2009 as

145 example, the annually averaged of SPM in surface waters varied from 58 g m^{-3} at the upstream limit of the estuary

146 to about 600 g m^{-3} at the mouth area, and fell again to 57 g m^{-3} at the seaward limit of fresh water diffusion (Li et

147 al., 2012). Due to the different river discharges, the SPM of the Yangtze Estuary exhibits seasonal variations (Shen

148 et al., 2013), with SPM in the upper estuary (lower estuary) during flood season significantly higher (lower) than

149 that during the dry season. Over the past 37 years, SPM in the Yangtze Estuary demonstrated an overall declining

150 pattern (Luo et al., 2022), with SPM in the inner estuary responding most promptly (40.3% reduction) after the

151 operation of Three Gorges Dam. [Chl-a] also shows seasonal variations in the Yangtze Estuary, ranging from 0.03

152 to 3.10 mg m^{-3} and from 0.88 to 31.5 mg m^{-3} during spring and summer seasons of 2008, respectively (Shen et al.,

153 2010b). In addition, the Yangtze Estuary is an area with frequent outbreaks of algal blooms, with diatoms being

154 the most frequently reported group (Shen et al., 2019; Zhu et al., 2019).

155 Two Hydrological Stations in Chongming Island, Shanghai, China, namely Chongxi (longitude:121.193°E, lati-

156 tude:31.759°N) and Baozhen (longitude:121.609°E, latitude:31.520°N) have been sampled from 30 May to 8 June

157 in 2018 (Table 1).

158

159 **3. Data collection**

160 The dataset contains measurements of the turbidity and, if available, concomitant SPM, absorption and attenuation

161 coefficients, [Chl-a] and reflectance measurements are also included (Lavigne et al., 2002; https://doi.pan-

162 gaea.de/10.1594/PANGAEA.944313). An overview of the dataset, with the number of observations after quality

163 control for each site and parameter, is provided in Table 2. The measurement methodology for each parameter is

164 described below.

165 **3.1 Water-leaving reflectance**

166 Above-water reflectance was determined using three TriOS/RAMSES hyperspectral spectroradiometers, two spec-

167 troradiometers measure radiance and one irradiance. The same TriOS instruments from RBINS institute were used

168 for all campaigns except the ones which occurred in Argentina where only instruments from IAFE institute were

169 available. The spectrometers measure in the 350-950 nm range with a sampling interval of 3.3 nm and effective

170 spectral resolution of 10 nm. The instruments were mounted on a frame and placed in the bow of the vessels

171 (Belgian coastal zone and Spuikom) or fixed to a rail when measurements were made from pontoons (Gironde,

172 Chascomús and Rio de la Plata). Zenith angles of the sea- and sky-viewing radiance sensors were set to 40°. Prior

173 to each measurement, the azimuth angle of the sensors was adjusted to obtain a relative azimuth angle with respect

174 to the sun of 90°, either left or right to get the best unobstructed view of the water and minimize structure pertur-

175 bation when measuring from pontoons. Simultaneous upwelling water radiance (L_u), downwelling sky radiance

176 (L_{sky}) and downwelling irradiance (E_d) were collected every 10 s for 10 min. Data was acquired using MSDA-XE

177 software and radiometrically calibrated using the latest calibration update from annual laboratory calibration. Wa-

178 ter reflectance (ρ_w) was calculated following

179
$$\rho_w(\lambda) = \frac{L_u(\lambda) - \rho_{sky}L_{sky}(\lambda)}{E_d(\lambda)}\pi$$

180 Where ρ_{sky} is the air-sea interface reflection coefficient which is calculated based, when available, on wind speed

181 as in Ruddick et al. (2006) or set to a fixed value of 0.0256 when measured in estuaries from fixed pontoon con-

182 sidering that surface waves are fetch-limited and not related to wind speed. The data processing, including quality

183 control, are described in Ruddick et al. (2006).

184 **3.2 Turbidity**

185 Turbidity was measured with two handheld HACH 2100P/Q ISO turbidimeters from RBINS and IAFE institutions.

186 In the HYPERMAQ dataset, turbidity data measured with the instrument from IAFE were provided by default as

187 they cover the most of the campaigns. However, when turbidity data from IAFE instrument were not available

188 (Belgian coastal waters, April 2018 and Spuikom April 2018), the values obtained with the instrument of the

189 RBINS were used. Figure 2 shows the good consistency of both instruments (r^2=0.99). Water samples were col-

190 lected from the surface with a bucket or from subsurface with a NISKIN bottle for measurements in coastal waters.

191 A 10 mL vial was filled and turbidity was determined in Formazin Nephelometric Unit (FNU) with the ratio of

192 light scattered at 90° compared to the transmitted light at 860 nm. Turbidity was recorded in triplicates and the

193 median value was used. Turbidimeters were controlled with standards STABCAL Stabilized Formazin Turbidity

194 of 0.1, 20, 100 and 800 FNU before and after each campaign.

195 In water turbidity was also measured with an OBS501 (OBS hereafter) using a CR200 data logger. Turbidity

196 measurements are derived from back-scattering with a field-of-view ranging from 125 to 170 degree and 90-degree

197 side-scattering of a signal emitted at 850 nm and data are provided in Formazin Backscatter Unit (FBU) and in

198 Formazin Nephelometric Unit (FNU), respectively. When deployed from a pier, OBS was continuously recording

199 data at subsurface throughout the whole day and values corresponding to specific stations were extracted from the

200 time-series in a time-window of 10 minutes centered on the timing of the radiometric measurement and water

201 sampling. When deployed from a boat, the OBS was maintained at subsurface (1 m depth) for at least 5 minutes.

202 Then, from a visual check, leading and trailing data of each time-series were removed and the central values were

203 averaged to obtain a final value.

204 **3.3 *In situ* absorption,beam attenuation and scattering coefficients**

205 The underwater absorption- and attenuation-meter (AC-9, WETLabs, Inc.) used was modified to cover the visible

206 and near-infrared (NIR; 700to 900 nm) spectral regions. It was designed with three visible (centered at 440 nm,

207 555 nm and 630 nm) and six NIR (centered at 715 nm, 730 nm, 750 nm, 767nm, 820 nm and 870 nm) spectral

208 channels, and a short pathlength (10 cm) appropriate for turbid coastal waters. At the sampling sites, the AC-9

209 sensor was either deployed within the water column using an electrical water pump (SBE, SeaBird, Inc.) or used

210 as a bench photometer passing the water samples right after collection through the tubes by gravimetry. The AC-

211 9 data recorded just below the water surface were averaged over the last minute of acquisition to obtain the mean

212 attenuation and absorption spectra for each station. Temperature and salinity corrections were applied as recom-

213 mended by the manufacturer. As in Doxaran et al. (2007), the residual scattering effects on absorption

214 measurements were corrected by applying the "proportional" method using 870 nm as the reference wavelength.
215 The scattering coefficient was calculated as the difference between the measured beam attenuation coefficient, c_{nw},
216 corrected for temperature and salinity effects, and the absorption coefficient, a_{nw}, corrected for temperature, salin-
217 ity and scattering effects. Those attenuation and absorption coefficients were referenced to pure water (non-water,
218 subscript "nw"), so that the scattering coefficient obtained by difference corresponds to the scattering coefficient
219 of marine particulates, b_p in m^{-1}. Small bubbles can contribute to the measured attenuation and scattering, but in
220 turbid systems particles dominate the signal. One of the main issues encountered when sampling highly turbid
221 waters was the saturation of the measured absorption and/or attenuation coefficients, which sometimes occurred
222 at short visible wavelengths and even in near-infrared bands in the case of extremely turbid waters. This saturation
223 was easily detected and the corresponding spectra were systematically removed from the dataset.

224 When possible, after AC-9 data measurements, the water sample collected was directly filtered through disc filters
225 (pore size 0.2 μm, Whatman). As in Doxaran et al. (2009b), the tube was rinsed twice with Milli-Q water and once
226 with the filtrate, and then filled with the filtrate. The absorption signal of the filtrate was measured, providing
227 a_{CDOM} in m^{-1}after applying corrections for temperature and salinity. The absorption coefficient of suspended par-
228 ticles (a_p, in m^{-1}) was finally calculated by subtracting the signal from the non-water absorption coefficient.

229 **3.4 Concentration of Suspended Particulate Matter and Suspended Inorganic Particulate Matter**

230 SPM concentration was determined gravimetrically following the protocol of Tilstone et al. (2002) which is based
231 on Van der Linde (1998).Water was sampled from the surface (maximum 2m depth) with a NISKIN bottle on
232 board the RV Simon Stevin or with a bucket in estuarine and inland waters. A sufficient volume of water was
233 filtered on a pre-ashed GF/F filter and conserved at -20°C before analysis. The volume filtrated was determined
234 as a function of the turbidity following recommendations of Neukermans et al. (2012). Inorganic suspended par-
235 ticulate matter (SPIM) was also calculated in all campaigns except in the Yangtze river. All the SPM measurements
236 have been conducted with 3 replicates to assess variability except for the campaigns in the Yangtze Estuary where
237 only one sample has been measured per each station. Filters were dried at 75°C for 24 hours and weighed in order
238 to determine the suspended matter concentration (SPM, in g m^{-3}). For SPIM measurements, filters were then
239 burned at 450°C for 4 hours to remove the organic part, and weighed again to estimate the suspended inorganic
240 particulate concentration (SPIM, in g m^{-3}).

241 **3.5 Chlorophyll-*a*and other pigment concentrations**

242 Phytoplankton pigments including [Chl-a] were determined using High Performance Liquid Chromatography
243 (HPLC) following the protocol of Van Heukelem and Thomas (2001) in campaigns in the Belgian coastal waters,
244 the Spuikom and the Gironde.In Belgian coastal waters, measurements were provided by the LifeWatchBE
245 sampling campaigns (Mortelmans et al., 2019, Flanders Marine Institute, 2021) of VLIZ. Pigment standards were
246 acquired from the Danish Hydrographic Institute (DHI). In the Gironde, the analysis of pigments were performed
247 by the SAPIGH analytical plateform of the "Institut de la Mer de Villefranche" (CNRS-France). In the Argentinian
248 campaigns [Chl-a] was determined spectrophotometrically using hot ethanol (60-70 °C) (Jespersen and

249 Christoffersen 1987). As for turbidity and SPM, water samples have been collected from surface water with a

250 bucket in inland waters or subsurface waters with a NISKIN in sea water.

251 **4. Results and discussions**

252 **4.1 SPM and turbidity results**

253 In the HYPERMAQ dataset SPM ranges between 1 g m^{-3} and 474 g m^{-3} (Table 3) and turbidity measured from

254 HACH and OBS (side-scattering measurements) ranges between 0.9 and 771 FNU and between 0.2 and 632 FNU

255 respectively. A very good relationship is observed between SPM and turbidity which almost follows the 1:1 line

256 for both instruments (Figure 3). A linear model between both parameters gives very good coefficients of determi-

257 nation ($R^2 = 0.98$ for HACH and $R^2 = 0.95$ for OBS) and slopes (0.92 for HACH and 0.86 for OBS). However, we

258 can notice that for very high turbidity (> 500 FNU), turbidity values measured by HACH tends be slightly higher

259 than SPM values (Figure 3A) but not OBS turbidity values. As expected from previous results, when comparing

260 side scattering turbidity obtained from OBS and turbidity measured by HACH, a good relationship is retrieved

261 (Figure 4A) with a R^2 of 0.96 and a slope of 0.84. Despite larger variability for very high turbidity, these results

262 confirm that OBS is a good tool for continuous measurements of turbidity in turbid environments.

263 The ratio of the side scattering versus the back scattering derived from OBS measurements has a particular interest

264 as it can provide information on the size and properties of the particles, e.g higher ratio could be explained by

265 larger particles (Nechad et al., 2016). In the HYPERMAQ dataset this ratio (Figure 4B) displayed a very high

266 variability in low turbidity environments and an increasing slope for high turbidity environments (i.e. Pauillac) as

267 also observed by Nechad et al. (2016). The very high variability when turbidity is low is explained by the strong

268 impact of uncertainty on low back scattering values in the ratio calculation. In Figure 4B, it can be observed that

269 the side scattering versus back scattering ratio varies significantly between and within sampled sites. For instance,

270 this ratio is higher in the Gironde Estuary at Le Verdon than in the Spuikom lagoon. It seems also to be higher in

271 the Río de la Plata and in the Gironde at Pauillac than in the Chascomús lake, though the Río de la Plata showed

272 high variability. Finally, the median ratio of the whole dataset is 1.77 which is close to the mean value of 1.72

273 found in Nechad et al. (2016) in turbid waters.

274 **4.2 Chl-a and other pigments concentrations**

275 [Chl-a] are extremely variable within HYPERMAQ test sites with values ranging between 0.91 mg m^{-3} in the

276 Gironde Estuary at Le Verdon and180.7 mg m^{-3} in the Chascomùs lake, although most of the observations are

277 within the range of 3 mg m^{-3} to 10 mg m^{-3} (Table 4). In addition, very high variability is observed within Belgian

278 waters and Spuikom, with [Chl-a] values ranging by a factor 10. This variability is mainly due to the fact these

279 study areas have been sampled in two different seasons (i.e. spring and summer).

280 Phytoplankton pigments derived from HPLC analysis were available in the Gironde Estuary, in the Belgian coastal

281 waters and in the Spuikom. The relative contribution of some key pigments for phytoplankton groups identification

282 (Uitz et al., 2006; Mackey et al., 1996) are represented on Figure 5. In the Gironde Estuary, at Le Verdon, signif-

283 icant concentration of fucoxanthin, peridin and chlorophyll-b are observed suggesting that diatoms, dinoflagellates

284   and chlorophytes are co-existing at similar levels. However, at Pauillac where phytoplankton biomass is higher
285   (Table 4), the high concentration of fucoxanthin suggests that planktonic assemblages were dominated by diatoms.
286   In Belgian waters, high value of fucoxanthin is also observed. This pattern was expected as fucoxanthin charac-
287   terized the two phytoplankton groups which are dominant during spring and summer in the Southern North Sea:
288   diatoms and the prymnesiophyte *Phaeocystisglobosa* (Lancelot et al., 2005). The last one is also characterized by
289   the presence of chlorophyll-c_3. In the Spuikom, fucoxanthin and chlorophyll-b show high concentrations indicating
290   an important proportion of diatoms and chlorophytes.

291   **4.3 Absorption and attenuation coefficients**

292   Very wide ranges of light absorption and attenuation coefficients were measured as representative of low to ex-
293   tremely turbid waters. As expected in CDOM- and sediment-rich waters, the spectral variations of the non-water
294   absorption coefficients were closely following an exponential function, with decreasing values from short visible
295   to near-infrared wavelengths (Figure 6A). The respective contributions of CDOM and suspended particles to light
296   absorption at 440 nm (Figure 7) were observed to vary from 20 % to 40% for CDOM and hence from 60 % to 80%
297   for suspended particles, which could be expected in productive waters strongly influenced by sediment inputs from
298   rivers and resuspension effects.
299   The spectral variations of the non-water attenuation coefficients (c_{nw}, Figure 6B) showed a smooth decrease with
300   increasing wavelengths, closely following the power-law function with varying slopes. These variations of the
301   spectral slope are expected to be representative of different particle size distributions due to the combined influ-
302   ences of wind-driven and tidal currents, and to the mixing between mineral-rich (sediments) and organic-rich
303   (phytoplankton) particles.

304   **4.4 Water reflectance**

305   The large diversity of water-leaving reflectance spectra is displayed in Figure 8. Maximum reflectance in each
306   spectrum varies from less than 0.02 on some spectra of the Belgian coastal waters to more than 0.15 in the Gironde
307   Estuary at Pauillac. Shapes of the spectra are also very variable. The mark of strong chlorophyll-a absorption
308   around 670 nm is well observed in the Chascomús and Spuikom lakes as well as in some spectra of the Belgian
309   coastal waters. The two extremely turbid sampling stations, the Rio de la Plata and the Gironde at Pauillac, show
310   some similarities in their spectral shapes although a large variability is observed at Pauillac due to a larger impact
311   of tides.
312   The relationship of water reflectance at 645 and 860 nm and turbidity (Figure 9) shows expected patterns with a
313   saturation of the reflectance at 645 nm when turbidity is higher than 200 FNU (Luo et al., 2018). Indeed, for these
314   extreme turbidity values the band at 860 nm shows a more linear relationship.

315   **5. Conclusion**

316   Coastal and inland waters strongly interact with human activities. Some of these activities, like fisheries or tourism,
317   rely on a good ecological status whereas the same activities but also others like farming, industry or urbanization

318 tend to affect water quality. Hence, monitoring these waters is extremely important and for that optical remote
319 sensing is a valuable tool as it allows a large spatial and temporal coverage. However, it is still challenging to
320 retrieve biogeochemical parameters in complex case 2 waters (Odermatt et al., 2012) because the transfer of light
321 in water is affected by temporally and spatially variable inputs of CDOM and terrestrial sediments. To help the
322 scientific community to build comprehensive database for the development of algorithms, the HYPERMAQ da-
323 taset provides data for six different studies areas with SPM and [Chl-a] ranging from moderate to extremely turbid
324 and productive, and located over three continents (i.e. Europe, South America and Asia). The HYPERMAQ dataset
325 includes big river estuaries characterized by high turbidity, inland lagoons with productivity ranging from moder-
326 ate to extreme and finally Belgian coastal waters in the North Sea characterized by the high spatio-temporal vari-
327 ability of optical properties (Vantrepotte et al., 2012). The parameters shared in the HYPERMAQ dataset include
328 descriptors of biogeochemical conditions (i.e. [Chl-a], SPM, turbidity) as well as AOPs (i.e. water reflectance) and
329 IOPs (a_{nw} and c_{nw}). Although this dataset does not aim to cover the whole variability of case 2 waters, it provides
330 valuable information to describe turbid and even extremely turbid waters and has the potential to help the devel-
331 opment of remote sensing algorithms. It can also contribute to the production of a larger optical database, based
332 on in situ measurements for a comprehensive description of case 2 waters.
333

Data availability

335 Data is available from Lavigne et al. (2022), hosted at PANGAEA (http://www.pangaea.de) under the doi:
336 https://doi.pangaea.de/10.1594/PANGAEA.944313.The HYPERMAQ dataset is subdivided into 10 sub-datasets
337 with their own DOI: absorptions and attenuation data (https://doi.pangaea.de/10.1594/PANGAEA.944361), Chl-
338 a concentration, turbidity and organic and inorganic sediments concentrations (https://doi.pan-
339 gaea.de/10.1594/PANGAEA.944364), pigment concentrations (https://doi.pangaea.de/10.1594/PAN-
340 GAEA.944321), spectral downwelling irradiance (https://doi.pangaea.de/10.1594/PANGAEA.944311) and its
341 standard deviation (https://doi.pangaea.de/10.1594/PANGAEA.944312), downwellingsky radiance
342 (https://doi.pangaea.de/10.1594/PANGAEA.944380)and its standard deviation (https://doi.pan-
343 gaea.de/10.1594/PANGAEA.944385), water downwelling radiance (https://doi.pangaea.de/10.1594/PAN-
344 GAEA.944369)and its standard deviation (https://doi.pangaea.de/10.1594/PANGAEA.944371) and finally water
345 reflectance (https://doi.pangaea.de/10.1594/PANGAEA.944474)and its standard deviation (https://doi.pan-
346 gaea.de/10.1594/PANGAEA.944475).

Author contributions

348 HL, AD, DD, FS, AC, XS, JIG, RP, MB, QV and KR participated to one or more field campaigns. Data processing
349 has been made by HL, AD and JIG (turbidity), DD (absorption), KR, MB, QV, RP, AD (water reflectance), AC,
350 AD, DD, FS, KS (chlorophyll-a, pigments and SPM). HL, DD, AD have compiled data and created the final
351 dataset. All authors participated to manuscript redaction and revision.

352 **Competing interests.**

353 The authors declare that they have no conflict of interest.

354 **Acknowledgements**

355 This work has been founded and promoted by the Research programme for earth observation 580 STEREO III
356 HYPERMAQ project (contract nr SR/00/335).Flemish LifeWatch BE programme, funding by FWO, is thanks for
357 its contribution to the water sampling in the Belgian Coastal Zone.We thank VLIZ for providing the Zeekat and
358 shiptime on the RV Simon Stevin and her crew for their support during sampling. Inland water sampling in
359 Belgium was also founded by the Belspo PONDER (SR/00/325) project. The SAPIGH analytical plateform of the
360 "Institut de la Mer de Villefranche" (CNRS-France) is thanks for having performed the analysis of pigments in the
361 Gironde. NASA, USGS, ESA and EUMETSAT are thanks to offer a free access to Landsat 8 and Sentinel 2
362 images.

363 **References**

364 Abril, G., Etcheber, H., Le Hir, P., Bassoullet, P., Boutier, B., & Frankignoulle, M., Oxic/anoxic oscillations and
365 organic carbon mineralization in an estuarine maximum turbidity zone (The Gironde, France). Limnology and
366 Oceanography, 44 (5), 1304– 1315, 1999.

367 Aubriot, L., Zabaleta, B., Bordet, F., Sienra, D., Risso, J., Achkar, M., & Somma, A., Assessing the origin of a
368 massive cyanobacterial bloom in the Río de la Plata (2019): Towards an early warning system. Water Research,
369 181, 115944, 2020.

370 Castaing, P., &Allen, G.P.,Mechanisms of seaward escape of suspended sediment from the Gironde: a macrotidal
371 estuary in France. Marine Geology 40, 101–118, 1981.

372 Castagna, A., Amadei Martínez, L., Bogorad, M., Daveloose, I., Dassevile, R., Dierssen, H. M., Beck, M., Mor-
373 telmans, J., Lavigne, H., Dogliotti, A., Doxaran, D., Ruddick, K., Vyverman, W., &Sabbe, K., Optical and bioge-
374 ochemical properties of Belgian inland and coastal waters, Earth Syst. Sci. Data Discuss.
375 https://doi.org/10.5194/essd-2021-466, in press, 2022.

376 Chen, Z., Saito, Y., Hori, K., Zhao, Y., & Kitamura, A., Early Holocene mud-ridge formation in the Yangtze
377 offshore, China: a tidal-controlled estuarine pattern and sea-level implications. Marine Geology, 198(3-4), 245-
378 257, 2003.

379 Diovisalvi, N., Berasain, G., Unrein, F., Colautti, D., Fermani, P., Llames, M.E., Torremorel, A.M., Lagomarsino,
380 L., Pérez, G., Escaray, R., Bustingorry, J., Ferraro, M.&Zagarese, H. Chascomús: estructura y funcionamiento de
381 una laguna pampeana turbia. Ecología Austral 20, 115–127, 2010.

382 Diovisalvi, N., Salcedo Echeverry, G.E., Lagomarsino, L.&Zagarese, M.E.,Seasonal patterns and responses to an
383 extreme climate event of rotifers community in a shallow eutrophic Pampean lake. Hydrobiologia 1 (1), 13, 2014.

Dogliotti, A. I., Camiolo, M., Simionato, C., Jaureguizar, A. J., Guerrero, R. A., &Lasta, C. Á., First optical observations in the turbidity maximum zone in the Río de la Plata estuary: A challenge for atmospheric correction algorithms. Ocean Optics XXII (USA, 26 al 31 de octubre de 2014), 2014.

Dogliotti, A. I., Ruddick, K., & Guerrero, R.,Seasonal and inter-annual turbidity variability in the Río de la Plata from 15 years of MODIS: El Niño dilution effect. Estuarine, Coastal and Shelf Science, 182, 27-39, 2016.

Dogliotti, A. I., Gossn, J. I., Gonzalez, C., Yema, L., Sanchez, M., & O'Farrell, I. L., Evaluation of Multi-and Hyper-Spectral Chl-A Algorithms in the Río De La Plata Turbid Waters During a Cyanobacteria Bloom. In 2021 IEEE International Geoscience and Remote Sensing Symposium IGARSS (pp. 7442-7445). IEEE, 2021.

Doxaran, D., Froidefond, J.M., Lavender, S.J. &Castaing P., Spectral signature of highly turbid waters. Application with SPOT data to quantify suspended particulate matter concentrations. Remote Sensing of Environment, 81, 149-161, 2002.

Doxaran D., Babin M. &Leymarie,E., Near-infrared light scattering by particles in coastal waters. Optics Express, 15(20), 12834-12849, 2007.

Doxaran, D., Froidefond, J.M., Castaing,P. &Babin, M., Dynamics of the turbidity maximum zone in a macrotidal estuary (the Gironde, France): Observations from field and MODIS satellite data. Estuarine, Coastal and Shelf Science 81, 321–332, 2009a.

Doxaran, D., Ruddick, K., McKee, D., Gentili, B., Tailliez, D., Chami, M., Babin, M., Spectral variations of light scattering by marine particles in coastal waters, from the visible to the near infrared. Limnology and Oceanography, 54, 1257-1271, 2009b.

Flanders Marine Institute. (2021). LifeWatch observatory data: nutrient, pigment, suspended matter and secchi measurements in the Belgian Part of the North Sea, https://doi.org/10.14284/441, 2021.

Framiñan, M. B.,& Brown, O.B., Study of the Río de la Plata turbidity front: I. Spatial and temporal distribution. Continental ShelfResearch 16, 1259-1282.1996.

Hieronymi, M., Krasemann, H., Müller, D., Brockmann, C., Ruescas, A., Stelzer, K., ... &Regner, P. (2016). Ocean colour remote sensing of extreme case-2 waters. *spectrum*, *2*, 4.

Hieronymi, M., Müller, D., & Doerffer, R. (2017). The OLCI Neural Network Swarm (ONNS): a bio-geo-optical algorithm for open ocean and coastal waters. *Frontiers in Marine Science*, *4*, 140.

Irigoien, X., & Castel, J., Light limitation and distribution of chlorophyll pigments in a highly turbid estuary: the Gironde (SW France). Estuarine, Coastal and Shelf Science, 44, 507– 517, 1997.

Jespersen, A.M. &Christoffersen, K., Measurements of chlorophyll-a from phytoplankton using ethanol as extraction solvent. Archiv für Hydrobiologie 109: 445-454, 1987.

Lacroix, G., Ruddick, K., Ozer, J., & Lancelot, C., Modelling the impact of the Scheldt and Rhine/Meuse plumes on the salinity distribution in Belgian waters (southern North Sea). Journal of Sea Research, 52(3), 149-163, 2004.

Lancelot, C., Spitz, Y., Gypens, N., Ruddick, K., Becquevort, S., Rousseau, V., Lacroix, G. &Billen, G., Modelling diatom and Phaeocystis blooms and nutrient cycles in the Southern Bight of the North Sea: the MIRO model. Marine Ecology Progress Series, 289, 63-78, 2005.

420 Lavigne, H., Dogliotti, A.,Doxaran, D., Shen, F.,Castagna, A., Beck, B., Vanhellemont, Q., Sun, X.,Gossn, J. I.;

421 Pannimpullath, R.,Sabbe, K.,Vansteenwegen, D., Ruddick, K., The HYPERMAQ dataset. PANGAEA,

422 https://doi.pangaea.de/10.1594/PANGAEA.944313.2022

423 Li, P., Yang, S. L., Milliman, J. D., Xu, K. H., Qin, W. H., Wu, C. S., Y. P. Chen, & Shi, B. W.,Spatial, temporal,

424 and human-induced variations in suspended sediment concentration in the surface waters of the Yangtze Estuary

425 and adjacent coastal areas. Estuaries and Coasts, 35(5), 1316-1327. 2012.

426 Luo, W., Shen, F., He, Q., Cao, F., Zhao, H., & Li, M., Changes in suspended sediments in the Yangtze River

427 Estuary from 1984 to 2020: Responses to basin and estuarine engineering constructions. Science of The Total

428 Environment, 805, 150381, 2022.

429 Mackey, M. D., Mackey, D. J., Higgins, H. W., & Wright, S. W., CHEMTAX-a program for estimating class

430 abundances from chemical markers: application to HPLC measurements of phytoplankton. Marine Ecology Pro-

431 gress Series, 144, 265-283, 1996.

432 Morel, A., &Maritorena, S., Bio-optical properties of oceanic waters: A reappraisal. Journal of Geophysical Re-

433 search: Oceans, 106(C4), 7163-7180, 2001.

434 Morel, A., &Prieur, L., Analysis of variations in ocean color 1. Limnology and oceanography, 22(4), 709-722,

435 1977.

436 Mortelmans, J., Deneudt, K., Cattrijsse, A., Beauchard, O., Daveloose, I., Vyverman, W., Vanaverbeke, J., Tim-

437 mermans, K., Peene, J., Roose, P., Knockaert, M., Chou, L., Sanders, R., Stinchcombe, M., Kimpe, P., Lammens,

438 S., Theetaert, H., Gkritzalis, T., Hernandez, F., and Mees, J.: Nutrient, pigment, suspended matter and turbidity

439 measurements in the Belgian part of the North Sea, Scientific Data, 22, https://doi.org/10.1038/s41597-019-0032-

440 7, 2019.

441 Muylaert, K., Gonzales, R., Franck, M., Lionard, M., Van der Zee, C., Cattrijsse, A., Sabbe, K., Chou, L.&Vyver-

442 man, W., Spatial variation in phytoplankton dynamics in the Belgian coastal zone of the North Sea studied by

443 microscopy, HPLC-CHEMTAX and underway fluorescence recordings. Journal of Sea Research, 55(4), 253-265,

444 2006.

445 Nechad, B., Dogliotti, A., Ruddick, K., &Doxaran, D., Particulate backscattering and suspended matter concen-

446 tration retrieval from remote-sensed turbidity in various coastal and riverine turbid waters. In Proceedings of ESA

447 living planet symposium, Prague (pp. 9-13), 2016.

448 Neukermans, G., Ruddick, K., Loisel, H., &Roose, P., Optimization and quality control of suspended particulate

449 matter concentration measurement using turbidity measurements. *Limnology and Oceanography: Methods*,

450 *10*(12), 1011-1023, 2012.

451 Odermatt, D., Gitelson, A., Brando, V. E., &Schaepman, M., Review of constituent retrieval in optically deep and

452 complex waters from satellite imagery. Remote sensing of environment, 118, 116-126, 2012.

453 Pérez, G.L., Llames, M.E., Lagomarsino, L., Zagarese, H., Seasonal variability of optical properties in a highly

454 turbid lake (Laguna Chascomús, Argentina). Photochemistry and Photobiology, 87: 659–670, 2011.

455 Ruddick, K. G., Cauwer, V. D., Park, Y. J., and Moore, G., Seaborne measurements of near infrared water-leaving

456 reflectance: The similarity spectrum for turbid waters, Limnol. Oceanogr., 51, 1167–1179, 2006.

457 Shen, F., Verhoef, W., Zhou, Y., Salama, M., & Liu, X., Satellite estimates of wide-range suspended sediment

458 concentrations in Changjiang (Yangtze) estuary using MERIS data. Estuaries and Coasts, 33(6), 1420-1429, 2010a

459 Shen, F., Zhou, Y. X., Li, D. J., Zhu, W. J., &Suhyb Salama, M., Medium resolution imaging spectrometer

460 (MERIS) estimation of chlorophyll-a concentration in the turbid sediment-laden waters of the Changjiang (Yang-

461 tze) Estuary. International Journal of Remote Sensing, 31(17-18), 4635-4650, 2010b.

462 Shen, F., Zhou, Y., Li, J., He, Q., & Verhoef, W., Remotely sensed variability of the suspended sediment concen-

463 tration and its response to decreased river discharge in the Yangtze estuary and adjacent coast. Continental Shelf

464 Research, 69, 52-61, 2013.

465 Shen, F., Tang, R., Sun, X., & Liu, D., Simple methods for satellite identification of algal blooms and species

466 using 10-year time series data from the East China Sea. Remote Sensing of Environment, 235, 111484, 2019.

467 Tilstone, G. H., Moore, G. F., Sørensen, K., Doerffer, R., &Røttgers, R., REVAMP Protocols. REVAMP metho-

468 dologies – EVG1 – CT – 2001 - 00049. http://envisat.esa.int/workshops/mavt_2003/MAVT-2003_802_RE-

469 VAMPprotocols3.pdf, 2002.

470 Torremorell, A., J. Bustigorry, R. Escaray&Zagarese, H. E., Seasonal dynamics of a large, shallow lake, laguna

471 Chascomús: the role of light limitation and other physical variables. Limnologica 37: 100–108, 2007.

472 Torremorell, A., M. E. Llames, G. L. Pérez, R. Escaray, J. Bustingorry&Zagarese, H. E., Annual patterns of phy-

473 toplankton density and primary production in a large, shallow lake: the central role of light. Freshwater Biology

474 54: 437–449, 2009.

475 Uitz, J., Claustre, H., Morel, A., & Hooker, S. B. Vertical distribution of phytoplankton communities in open

476 ocean: An assessment based on surface chlorophyll. Journal of Geophysical Research: Oceans, 111(C8), 2006.

477 Van der Linde, D. W., Protocol for the determination of total suspended matter in oceans and coastal zones. Joint

478 Research Centre, Ispra. Technical note I.98.182, 1998.

479 Van Heukelem, L., & Thomas, C. S., Computer-assisted high-performance liquid chromatography method devel-

480 opment with applications to the isolation and analysis of phytoplankton pigments. *Journal of Chromatography A*,

481 *910*(1), 31-49, 2001.

482 Vantrepotte, V., Loisel, H., Dessailly, D., &Mériaux, X.,Optical classification of contrasted coastal waters. Remote

483 Sensing of Environment, 123, 306-323, 2012.

484 Zhu, W., Wang, M., & Zhang, B., The effects of urbanization on PM2. 5 concentrations in China's Yangtze River

485 Economic Belt: New evidence from spatial econometric analysis. Journal of cleaner production, 239, 118065,

486 2019.

487   **Table 1: Date, locationand platform of the campaigns.**

488

Campaign	Date	Platform	Latitude (deg)	Longitude (deg)
Spuikom	19 April 2018, 23,24 and 27 July 2018	Inflatable boat	51.23	2.95
Belgian Coastal waters	23-25 April 2018, 25-26July2018	RV Simon Stevin	51.18-51.59	2.50-3.15
Gironde (Pauillac)	17 and 19 Sept. 2018	Harbor	45.1975	-0.7422
Gironde (Le Verdon)	18 and 20 Sept. 2018	Pier	45.5438	-1.042
Chascomùs	9-10 April 2018	Pier	-35.5828	-58.0202
Rio de la Plata (Buenos Aires)	4-5 April 2018	Pier	-34.5609	-58.3988
Yangtze (Chongxi)	31 May, 1 and 3 June 2018	Pier	31.759	121.193
Yangtze (Baozhen)	4-8 June 2018	Pier	31.520	121.609

489

490   **Table 2: Number of observations for each sampling site. *also include pigments concentrations from HPLC.**

Campaign / Site	TriOS	TUR (HACH)	TUR (OBS)	a_{nw} - c_{nw} AC-9	SPM	[Chl-a]
Spuikom	27	27	23	11	17	17*
Belgian coastal waters	18	19	17	10	19	18*
Gironde - Pauillac	25	26	26	23	13	13*
Gironde – Le Verdon	21	25	25	24	12	12*
Chascomùs	5	5	5	5	5	3
Rio de la Plata- BA	16	22	22	18	10	10
Yangtze - Chongxi	-	16	-	-	16	-
Yangtze - Baozhen	-	37	-	29	37	-

491

492

493   **Table 3: Distribution of SPM (g m⁻³) in each sampling site.**

	SPM (g m⁻³)			
Campaign / Site	min	median	mean	max
Spuikom	2.06	3.16	3.93	8.40
Belgian coastal waters	1.02	4.49	9.63	62.04
Gironde - Pauillac	22.5	181	177	474
Gironde – Le Verdon	5.85	7.80	10.2	23.5
Chascomús	81.0	175	141	189
Rio de la Plata	49.3	71.7	74.0	93.8
Yangtze - Chongxi	27.2	42.2	44.8	66.4
Yangtze - Baozhen	23.6	52.8	53.6	138.4

494
495
496

497 **Table 4: Distribution of Chl-aconcentration (mg m⁻³) in each sampling site.**

498

	Chl-a (mg m⁻³)			
Campaign / Site	min	median	mean	max
Spuikom	2.40	9.16	10.64	22.70
Belgian coastal waters	1.99	6.33	7.49	17.36
Gironde - Pauillac	2.49	3.82	3.88	6.85
Gironde – Le Verdon	0.91	1.63	1.67	2.79
Chascomús	141.5	141.5	154.6	180.7
Rio de la Plata-BA	2.17	3.27	3.72	8.71
Yangtze - Chongxi	-	-	-	-
Yangtze - Baozhen	-	-	-	-

499

500

501

502

503
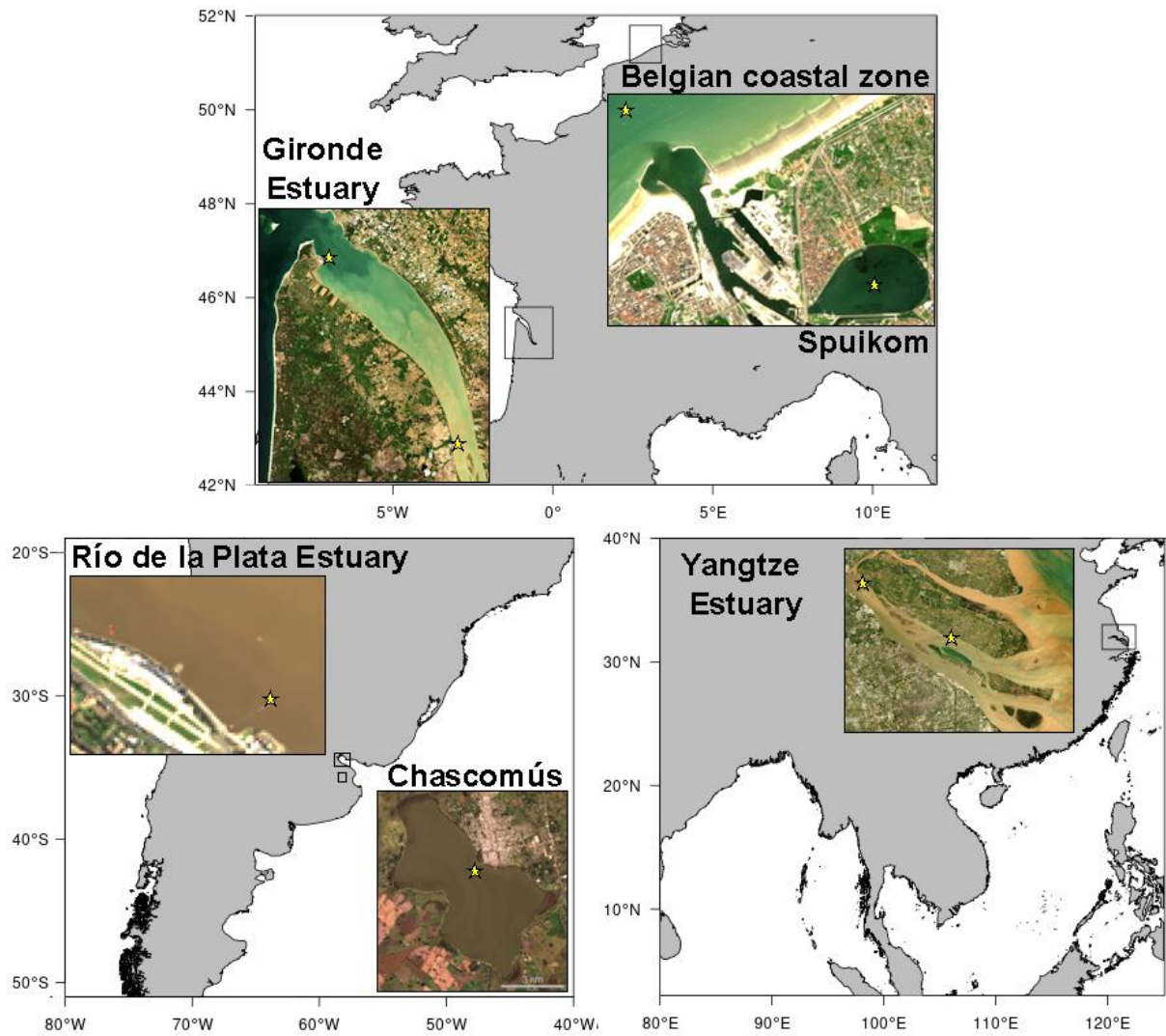
Figure 1: Locations of the study areas. Satellite images are coming from Landsat 8 OLI (Yangtze: image taken on 2021-04-29, Chascomùs: image taken on 10-05-2017, Rio de la Plata: image taken on 2014-08-13) and Sentinel 2B MSI (Belgian Coastal Zone: image taken on 2021-05-30, Gironde: image taken on 2021-05-03)

508

509

510
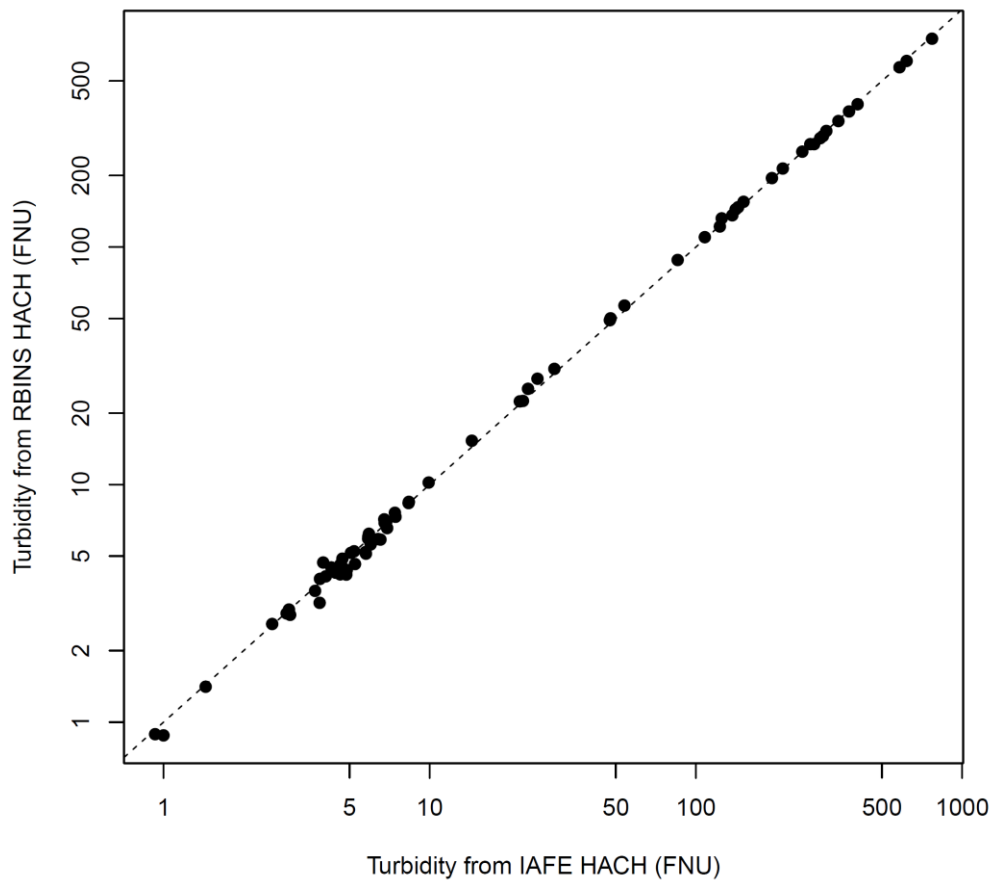
Figure 2: Comparison of simultaneous measurements of turbidity made from two different HACH instruments (r^2=0.99).

515
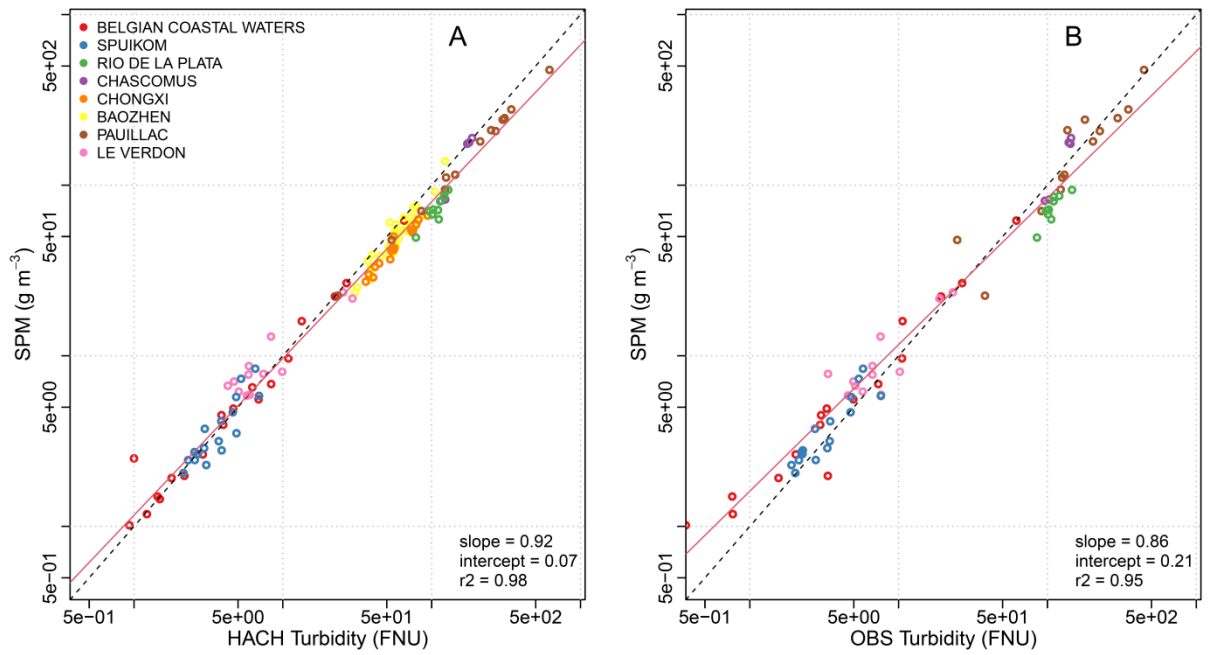
516

517 **Figure 3: SPM as a function of turbidity. Turbidity from OBS is given by the side-scattering measurement. The dotted**
518 **line is the 1:1 line and the red line represents the linear regression between SPM and turbidity.**

519

520
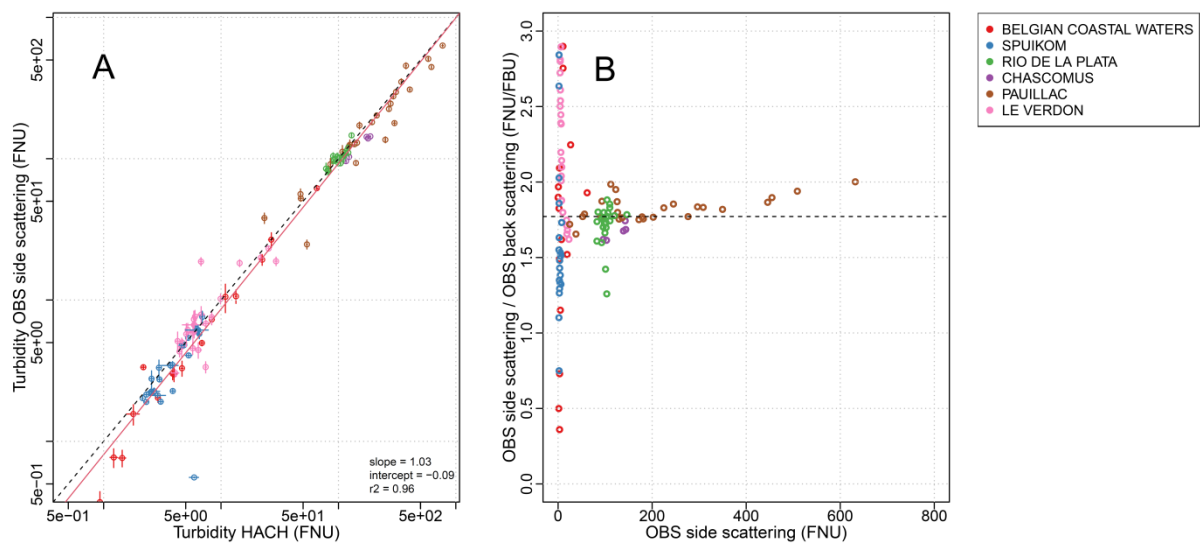
Figure 4: Turbidity measured by HACH instrument as a function of side-scattering turbidity measured by the OBS instrument (panel A). The red line shows the least squares regression between these variables. Panel B: ratio of the OBS side-scattering to backscattering ratio as a function of the OBS side-scattering. The horizontal dotted line represents the median value of the scattering ratio.

525

526

527
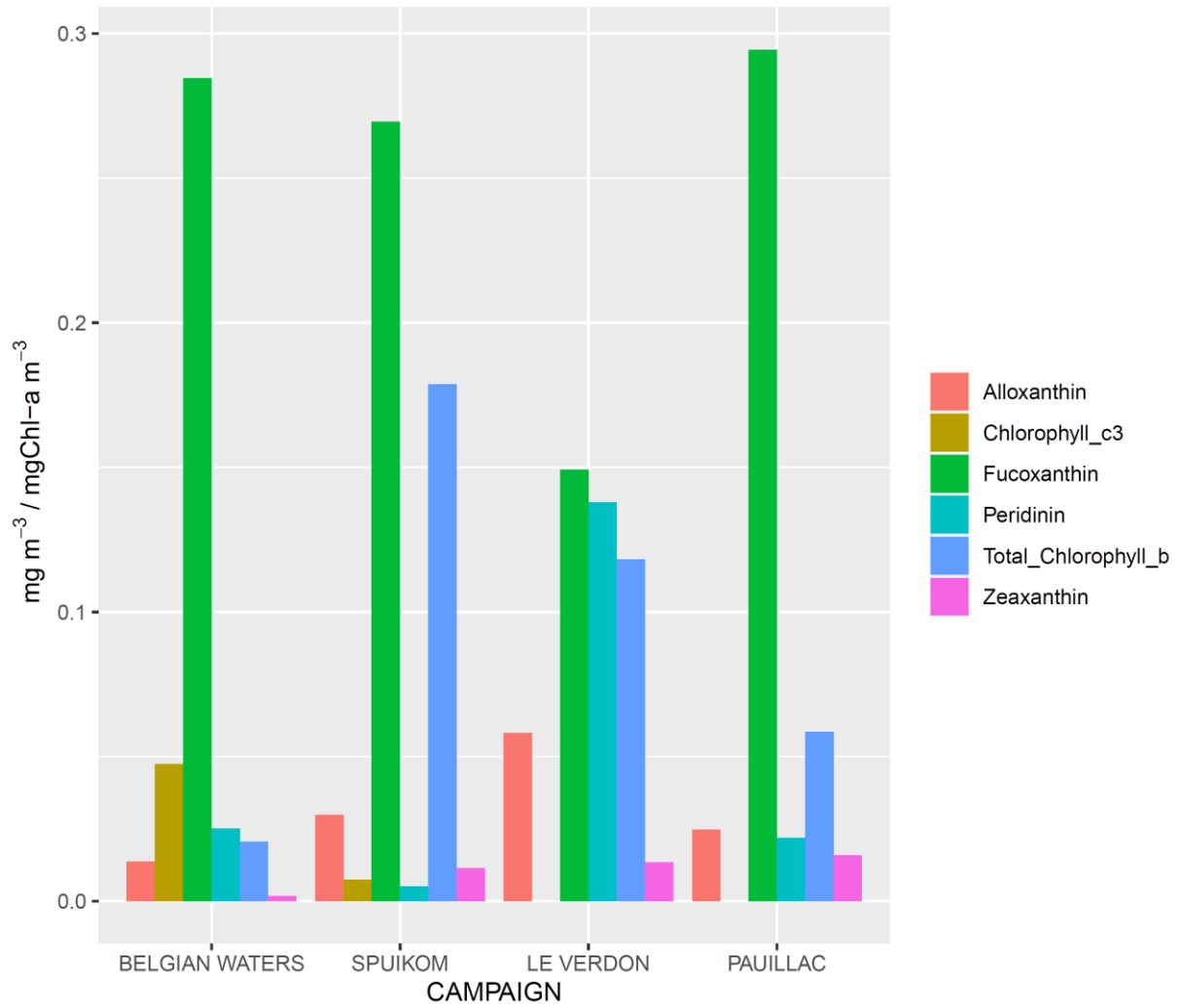
Figure 5: For each campaign, average concentration of alloxanthin, fucoxanthin, peridinin, chlorophyll c₃, zeaxanthin
and total chlorophyll b normalized by the concentration in chlorophyll-a

530
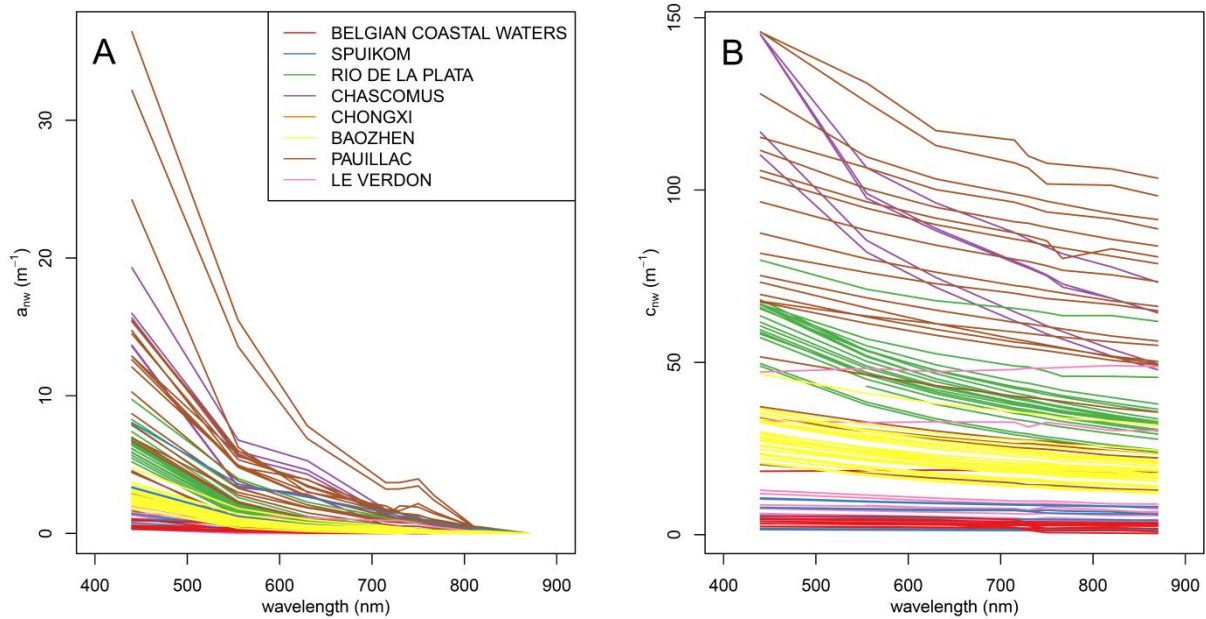
531

532 **Figure 6: Non-water absorption (panel A) and attenuation coefficients (panel B) measured with theAC-9 instrument.**

533
534
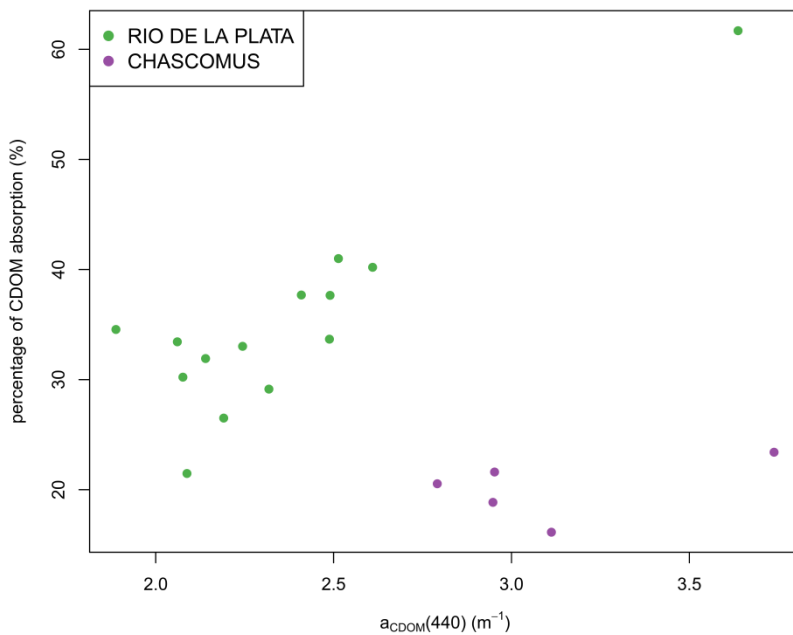
535
536 **Figure 7: Percentage of CDOM absorption as a function of a_CDOM(440). a_CDOM was only measured during two cam-**
537 **paigns.**
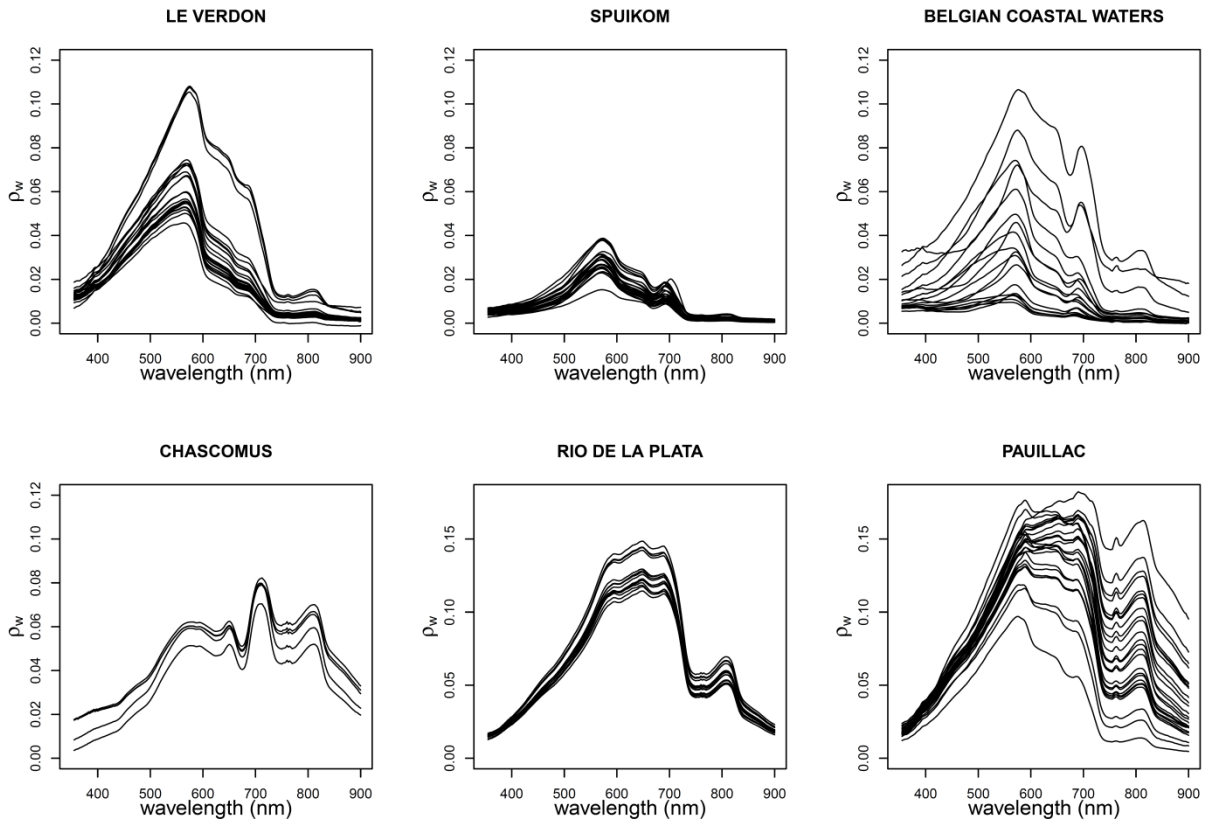
538
539 **Figure 8: Water reflectance spectra (unitless) from each sample site.**

540

541
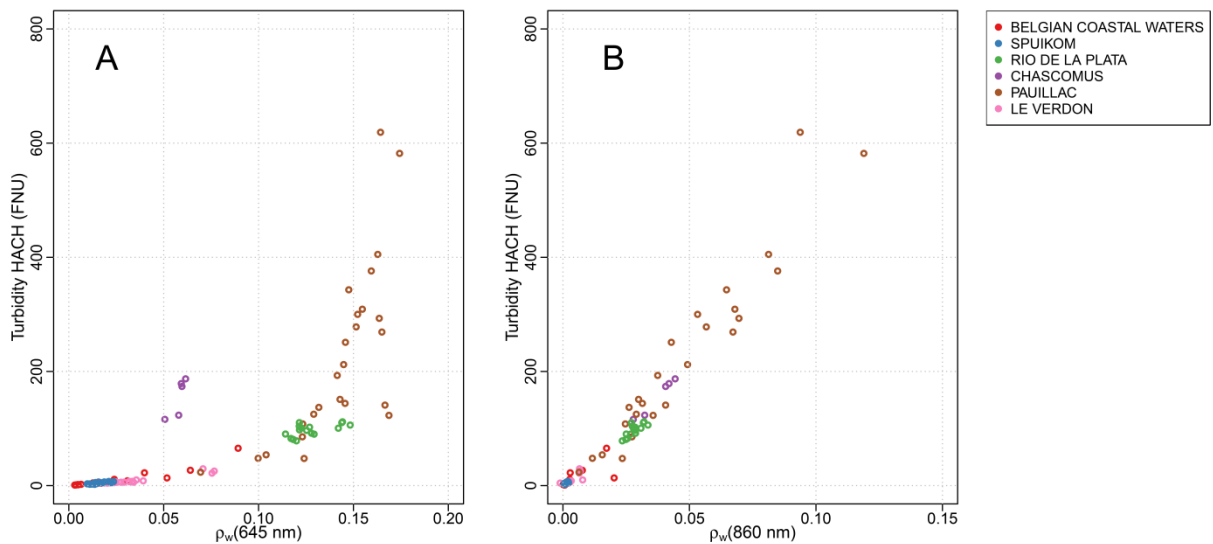
542
543 **Figure 9: Turbidity as a function of water reflectanceat 645 nm (panel A) and 850 nm (panel B). Black dotted line**
544 **represents the model of Nechad et al. (2009) between 0 and 100 FNU.**